Supplementary Material (ESI) for ***CrystEngComm 2020***.

Three water-stable luminescent two-dimensional Cd^{II}-based coordination polymers as sensors for highly sensitive and selective detection of $Cr_2O_7^{2-}$ and CrO_4^{2-} anions

Yong-Sheng Shi[a], Qing-Qing Xiao[a], Lianshe Fu[b], Guang-Hua Cui[a]*

[a]*College of Chemical Engineering, Hebei Key Laboratory for Environment Photocatalytic and Electrocatalytic Materials, North China University of Science and Technology, No. 21 Bohai Road, Caofeidian new-city, Tangshan, Hebei, 063210, P. R. China*

[b]*Department of Physics and CICECO-Aveiro Institute of Materials, University of Aveiro, 3810-193 Aveiro, Portugal*

*Corresponding author: Guang-Hua Cui

Fax: +86-315-8805462. Tel: +86-315-8805460

E-mail: tscghua@126.com.

Table Titles:

Table S1 Crystal data and structure refinements for the **1−3.**

Table S2 Selected bond lengths [Å] and angles [º] for the **1−3.**

Table S1 Crystal data and structure refinements for the **1**−**3.**

Cd-CPs	**1**	**2**	**3**
Chemical formula	$C_{30}H_{32.70}CdN_4O_{5.35}$	$C_{29}H_{27}CdN_5O_6$	$C_{33}H_{30}CdN_4O_4$
Formula weight	647.30	653.95	659.01
Crystal system	Triclinic	Triclinic	Monoclinic
Space group	*P*$\bar{1}$	*P*$\bar{1}$	*P2(1)/n*
a (Å)	10.349(2)	10.578(4)	11.369(6)
b (Å)	11.096(2)	10.841(5)	13.041(7)
c (Å)	13.621(3)	11.676(5)	18.032(10)
α (°)	111.687(3)	100.906(6)	90
β (°)	92.716(3)	100.575(6)	91.795(6)
γ (°)	95.370(3)	91.284(6)	90
V (Å^3)	1441.3(5)	1290.2(9)	2672(3)
Z	2	2	4
D_{calcd} (g/cm^3)	1.491	1.683	1.638
Absorption coefficient, mm^{-1}	0.804	0.903	0.866
F(000)	663	664	1344
Crystal size, mm	0.16 × 0.12 × 0.12	0.18 × 0.17 × 0.13	0.26 × 0.22 × 0.18
θ range, deg	1.615–27.535	1.810–27.536	1.927–27.592
Index range *h*, *k*, *l*	-13/10, -13/14, -17/17	-13/12, -12/14, -14/15	-13/14, -16/13, -21/23
Reflections collected	8808	7834	15550
Independent reflections (R_{int})	6355(0.0204)	5671(0.0528)	6087(0.0237)
Data/restraint/parameters	6355/0/357	5671/0/374	6087/0/383
Goodness-of-fit on F^2	0.932	1.012	1.061
Final R_1, wR_2 ($I > 2\sigma(I)$)	0.0361, 0.0922	0.0751, 0.1795	0.0247, 0.0726
Largest diff. peak and hole	0.576, -0.421	1.680, -2.480	0.331, -0.559

Table S2 Selected bond lengths [Å] and angles [º] for the **1**−**3.**

Parameter	Value	Parameter	Value
1			
Cd(1)-O(1)	2.229(2)	Cd(1)-O(2)A	2.366(2)
Cd(1)-O(3)B	2.372(2)	Cd(1)-O(4)B	2.388(2)
Cd(1)-N(1)	2.298(2)	Cd(1)-N(4)C	2.381(3)
O(1)-Cd(1)-O(2)A	91.27(8)	O(1)-Cd(1)-O(3)B	144.68(9)
O(1)-Cd(1)-O(4)B	91.18(9)	O(1)-Cd(1)-N(1)	120.82(9)
O(1)-Cd(1)-N(4)C	87.51(9)	O(2)A-Cd(1)-O(3)B	99.54(9)
O(2)A-Cd(1)-O(4)B	94.20(9)	O(2)A-Cd(1)-N(1)	87.42(9)
O(2)A-Cd(1)-N(4)C	171.77(8)	O(3)B-Cd(1)-O(4)B	54.77(8)
O(3)B-Cd(1)-N(1)	93.35(9)	O(3)B-Cd(1)-N(4)C	86.06(10)
O(4)B-Cd(1)-N(1)	147.94(9)	O(4)B-Cd(1)-N(4)C	93.96(10)
N(1)-Cd(1)-N(4)C	86.22(10)		
2			
Cd(1)-O(1)	2.153(5)	Cd(1)-O(3)A	2.497(5)
Cd(1)-O(4)A	2.278(5)	Cd(1)-O(3)C	2.805(6)
Cd(1)-N(1)	2.251(6)	Cd(1)-N(4)B	2.347(6)
O(1)-Cd(1)-O(3)A	117.89(2)	O(1)-Cd(1)-O(4)A	136.49(2)
O(1)-Cd(1)-O(3)C	73.32(2)	O(1)-Cd(1)-N(1)	117.07(2)
O(1)-Cd(1)-N(4)B	94.45(2)	O(3)A-Cd(1)-O(4)A	53.35(19)
O(3)A-Cd(1)-O(3)C	67.58(19)	O(3)A-Cd(1)-N(1)	93.34(2)
O(3)A-Cd(1)-N(4)B	133.71(19)	O(4)A-Cd(1)-O(3)C	120.78(2)
O(4)A-Cd(1)-N(1)	106.31(2)	O(4)A-Cd(1)-N(4)B	80.37(2)
O(3)C-Cd(1)-N(1)	71.00(2)	O(3)C-Cd(1)-N(4)B	158.45(19)
N(1)-Cd(1)-N(4)B	100.55(2)		
3			
Cd(1)-O(1)	2.305(2)	Cd(1)-O(2)	2.678(2)
Cd(1)-O(2)A	2.381(2)	Cd(1)-O(3)B	2.434(2)
Cd(1)-O(4)B	2.342(2)	Cd(1)-N(1)	2.287(2)
Cd(1)-N(4)A	2.336(2)		
O(1)-Cd(1)-O(2)	50.98(6)	O(1)-Cd(1)-O(2)A	130.90(6)
O(1)-Cd(1)-O(3)B	142.54(6)	O(1)-Cd(1)-O(4)B	89.27(7)
O(1)-Cd(1)-N(1)	92.77(7)	O(1)-Cd(1)-N(4)A	93.05(7)
O(2)-Cd(1)-O(2)A	80.27(6)	O(2)-Cd(1)-O(3)B	166.13(6)
O(2)-Cd(1)-O(4)B	139.63(6)	O(2)-Cd(1)-N(1)	82.94(6)
O(2)-Cd(1)-N(4)A	93.65(6)	O(2)A-Cd(1)-O(3)B	85.92(6)
O(2)A-Cd(1)-O(4)B	139.83(6)	O(2)A-Cd(1)-N(1)	85.77(7)
O(2)A-Cd(1)-N(4)A	83.49(7)	O(3)B-Cd(1)-O(4)B	54.24(6)
O(3)B-Cd(1)-N(1)	97.37(7)	O(3)B-Cd(1)-N(4)A	83.48(7)

O(4)B-Cd(1)-N(1)	93.77(7)	O(4)B-Cd(1)-N(4)A	95.46(7)
N(1)-Cd(1)-N(4)A	169.15(6)		

symmetry code: A = 1-*x*, 2-*y*, 1-*z*; B = 1+*x*, *y*, *z*; C = 1-*x*, 1-*y*, 1-*z* for **1**; A = *x*, 1+*y*, *z*; B = -1+*x*, *y*, *z*; C = 1-*x*, 1-*y*, 1-*z* for **2**; A = 1-*x*, 1-*y*, 1-*z*; B = -0.5+*x*, 1.5-*y*,-0.5+ *z* for **3.**

Fig. S1. (a) the binuclear $[Cd_2(L)_2]$ unit was formed by L ligands and Cd^{II} atoms; (b) The MIP^{2-} anions create a 1D infinite $[Cd(MIP)]_n$ chain by linking adjacent Cd^{II} ions in **1**; (c) the 3D supramolecular network of **1** formed by π–π stacking interactions (red dotted line).

Fig. S2. (a) one varying 1D chains, named as $[Cd(NTP)]_n$ is formed by H_2NTP ligands and Cd^{II} atoms in **2**; (b) one 1D "V" like chains $[Cd_2(L)_2]_n$ with the surrounding Cd^{II} centers in **2** (c) the 3D supramolecular network of **2** formed by π–π stacking interactions (red dotted line).

Fig. S3. (a) The 1,4-NDC^{2-} anions connect the adjacent Cd^{II} ions to form a two-dimensional layered structure in **3;** (b) The simplified layer of 1,4-NDC^{2-} anions and Cd^{II} ions is topologically described as a three-connected single-node **fes** topology network with dot symbol $\{4.8^2\}$; (c) the binuclear $[Cd_2(L)_2]$ unit was formed by L ligands and Cd^{II} atoms in **3**; (d) the 3D supramolecular network of **3** formed byπ–π stacking interactions (red dotted line).

Fig. S4. The infrared spectra of Cd-CPs **1**–**3.**

Fig. S5. The PXRD patterns of the bulk samples are consistent with the simulated ones of the single crystal structures in Cd-CPs **1**–**3.**

Fig. S6. TGA curves of Cd-CPs **1**–**3.**

Fig. S7. Luminescence emission spectra of L and **1-3** in the solid state.

Fig. S8. (a) Time-dependent emission spectra of **1** suspended in aqueous solutions; (b) Time-dependent emission spectra of **3** suspended in aqueous solutions.

Fig. S9. (a) PXRD patterns of **1** under simulated conditions; (b)PXRD patterns of **3**

under simulated conditions.

Fig. S10. (a) The change of the PXRD patterns of **1** in different pH solutions; (b) The change of PXRD patterns of **3** in different pH solutions.

Fig. S11. Fluorescence intensities of **2** in water with various potassium salts (5×10^{-4} mol/L)

Fig. S12. In **1**, the time required for the quenching efficiency of $Cr_2O_7^{2-}/CrO_4^{2-}$ anions to reach the maximum.

Fig. S13. In **3**, the time required for the quenching efficiency of $Cr_2O_7^{2-}/CrO_4^{2-}$ anions to reach the maximum.

Fig. S14. Comparison of the quenching efficiency of **1** and **3** for $Cr_2O_7^{2-}/CrO_4^{2-}$over three cycles.

Fig. S15. (a) The PXRD patterns of **1** sample was immersed in H_2O solution containing $Cr_2O_7^{2-}/CrO_4^{2-}$ anions and other common anions; (b)The PXRD patterns of **3** sample was immersed in H_2O solution containing $Cr_2O_7^{2-}/CrO_4^{2-}$ anions and other common anions.

Fig. S16. (a)The original infrared spectrum of **1**, and the infrared spectra measured after $Cr_2O_7^{2-}/CrO_4^{2-}$ detection of **1.** (b)The original infrared spectrum of **3**, and the infrared spectra measured after $Cr_2O_7^{2-}/CrO_4^{2-}$ detection of **3.**

Fig. S17. (a) Effects of pH on the fluorescence maxima of **1** + CrO_4^{2-} (circle) and **1** + $Cr_2O_7^{2-}$ (triangle). Solvent: H_2O (1:1, v/v); (b) Effects of pH on the fluorescence maxima of **3** + CrO_4^{2-} (circle) and **3** + $Cr_2O_7^{2-}$ (triangle). Solvent: H_2O (1:1, v/v).

Fig. S18. (a) The EDX patterns of **3**, **3** + CrO_4^{2-}, **3** + $Cr_2O_7^{2-}$, respectively; (b) The EDX patterns of **3**, **3** + CrO_4^{2-}, **3** + $Cr_2O_7^{2-}$, respectively.

Fig. S19. (a) Spectral overlap between the absorption spectrum of $Cr_2O_7^{2-}$anions and the excitation spectrum of **3**; (b) Spectral overlap between the absorption spectrum of $Cr_2O_7^{2-}$anions and the excitation spectrum of **3**.

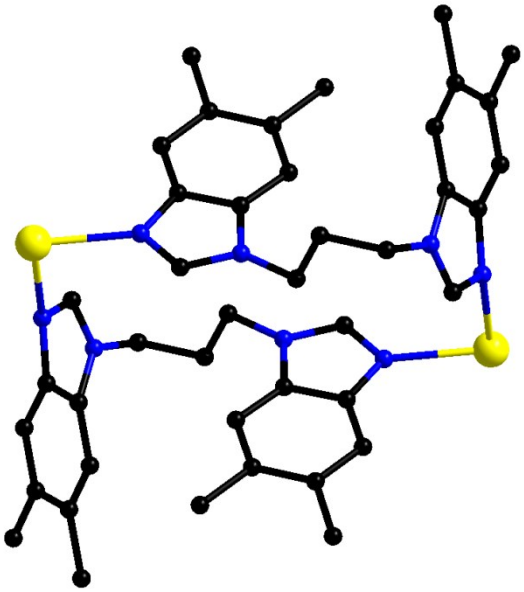

(a)

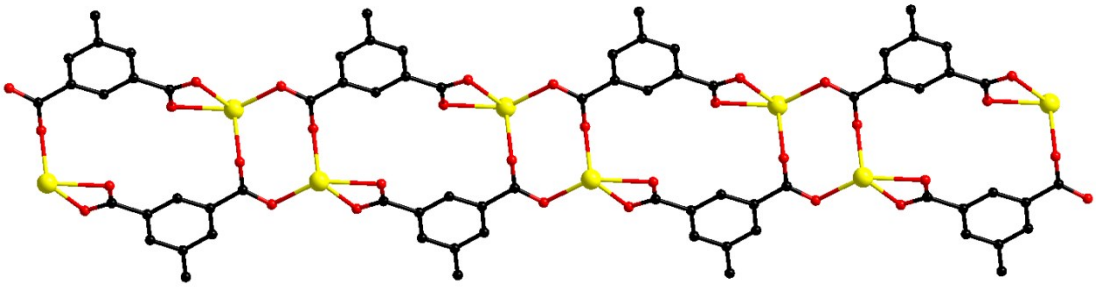

(b)

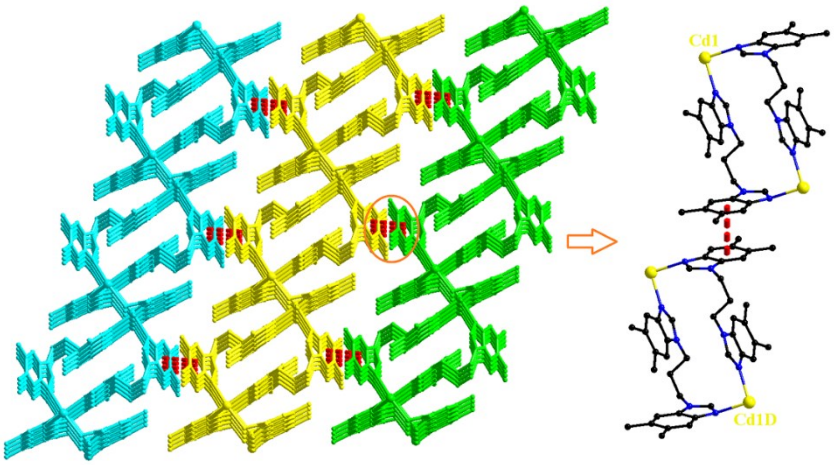

(c)

Fig. S1. (a) the binuclear $[Cd_2(L)_2]$ unit was formed by L ligands and Cd^{II} atoms; (b) The MIP^{2-} anions create a 1D infinite $[Cd(MIP)]_n$ chain by linking adjacent Cd^{II} ions in **1**; (c) the 3D supramolecular network of **1** formed by π–π stacking interactions (red dotted line).

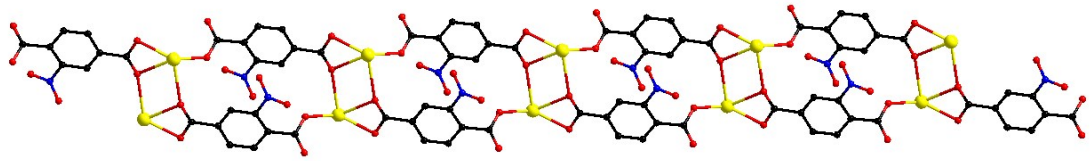

(a)

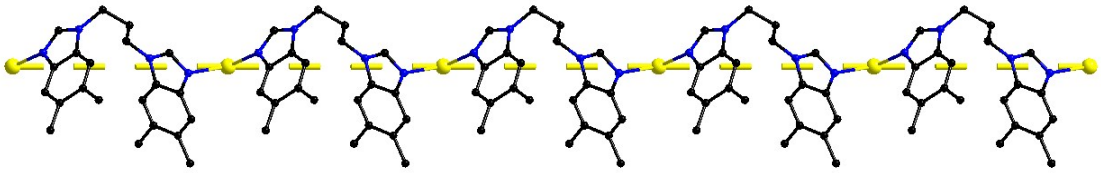

(b)

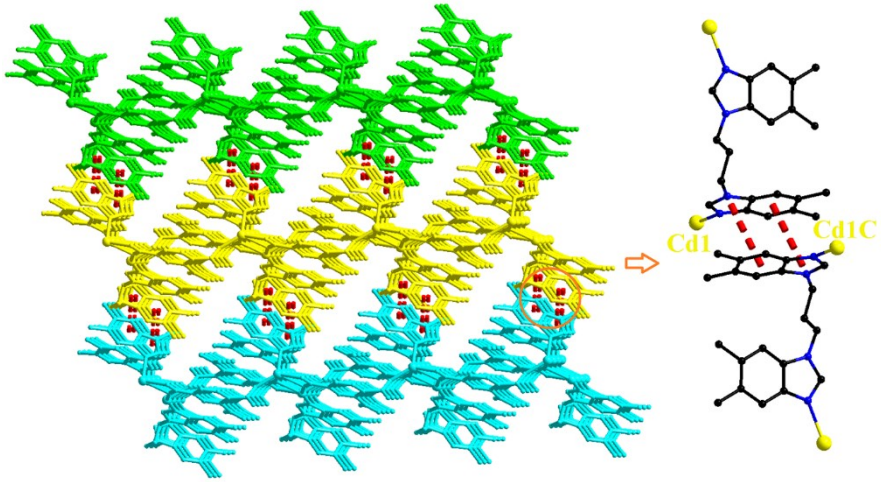

(c)

Fig. S2. (a) one varying 1D chains, named as $[Cd(NTP)]_n$ is formed by H_2NTP ligands and Cd^{II} atoms in **2**; (b) one 1D "V" like chains $[Cd_2(L)_2]_n$ with the surrounding Cd^{II} centers in **2** (c) the 3D supramolecular network of **2** formed byπ–π stacking interactions (red dotted line).

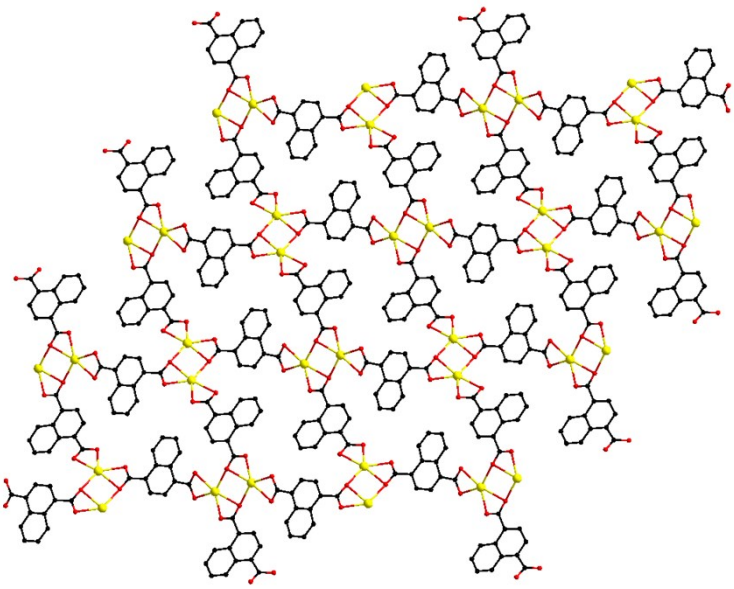

(a)

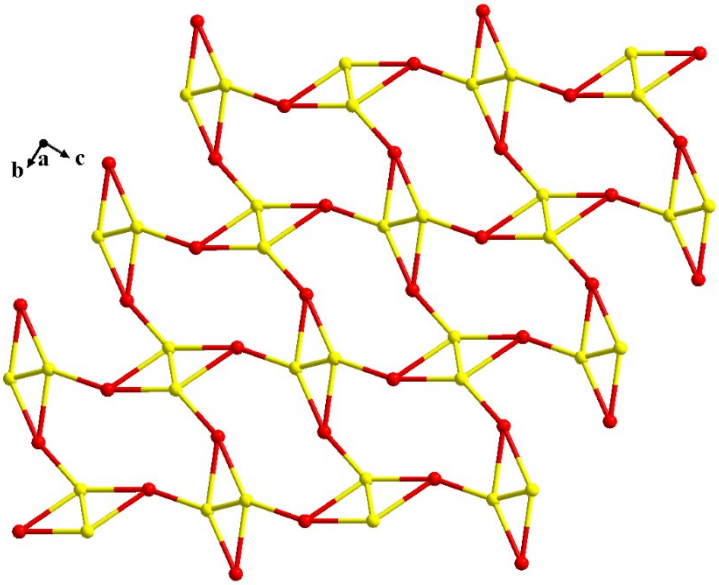

(b)

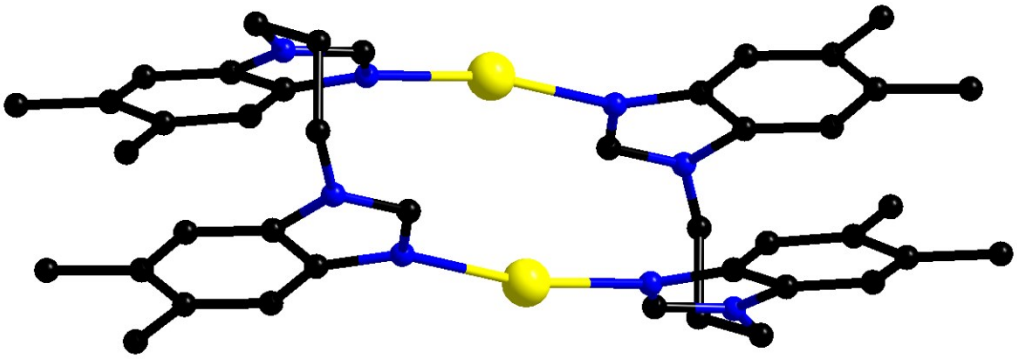

(c)

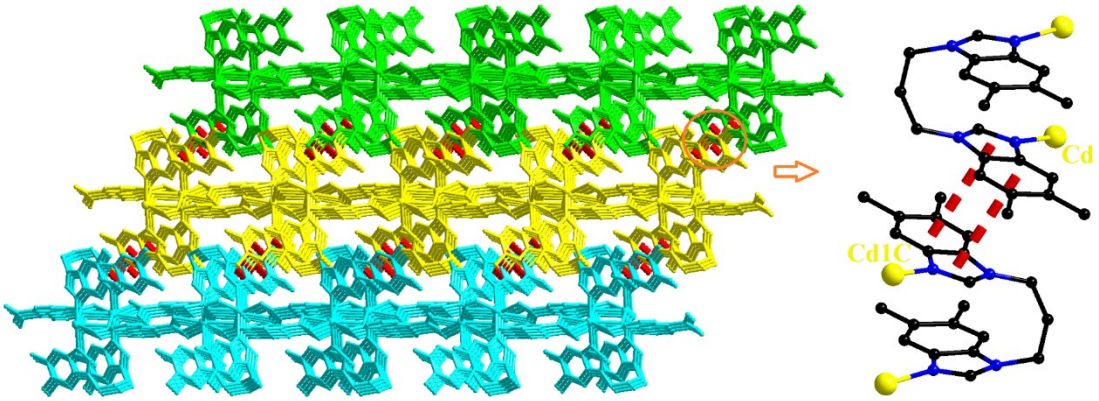

Fig. S3. (a) The 1,4-NDC^{2-} anions connect the adjacent Cd^{II} ions to form a two-dimensional layered structure in **3;** (b) The simplified layer of 1,4-NDC^{2-} anions and Cd^{II} ions is topologically described as a three-connected single-node **fes** topology network with dot symbol $\{4.8^2\}$; (c) the binuclear $[Cd_2(L)_2]$ unit was formed by L ligands and Cd^{II} atoms in **3**; (d) the 3D supramolecular network of **3** formed byπ–π stacking interactions (red dotted line).

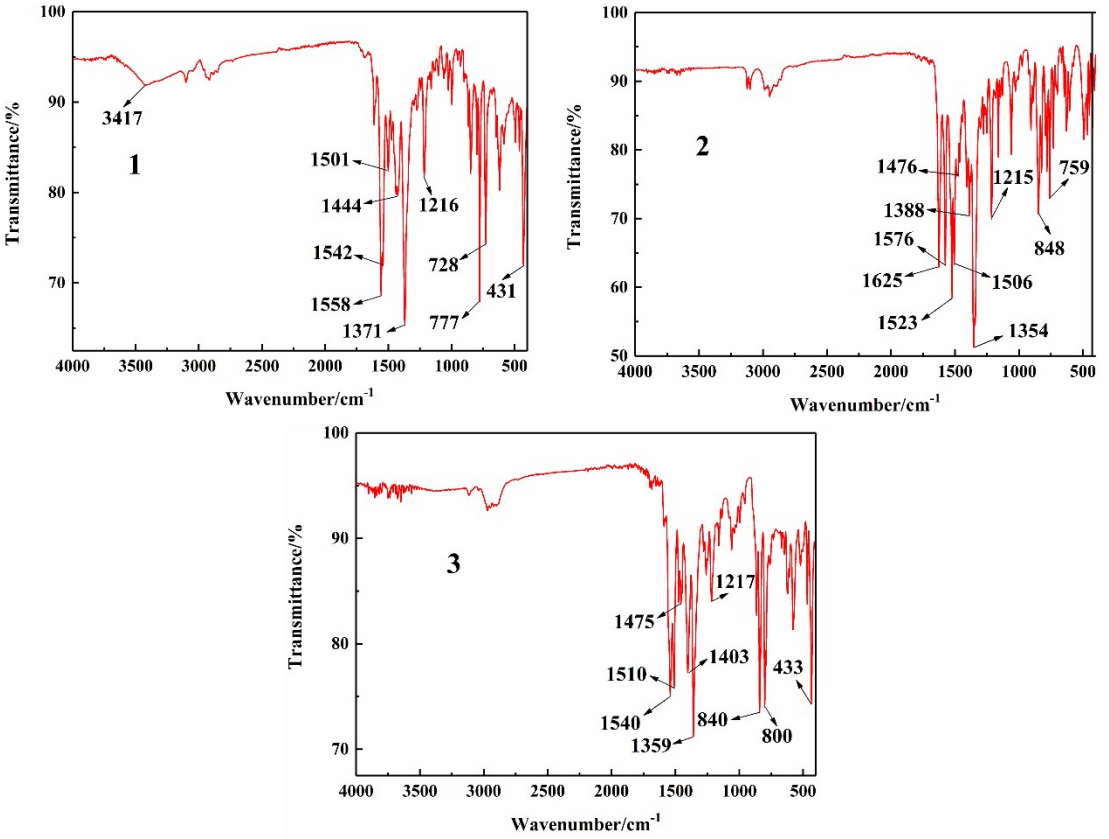

Fig. S4. The infrared spectra of Cd-CPs **1**–**3.**

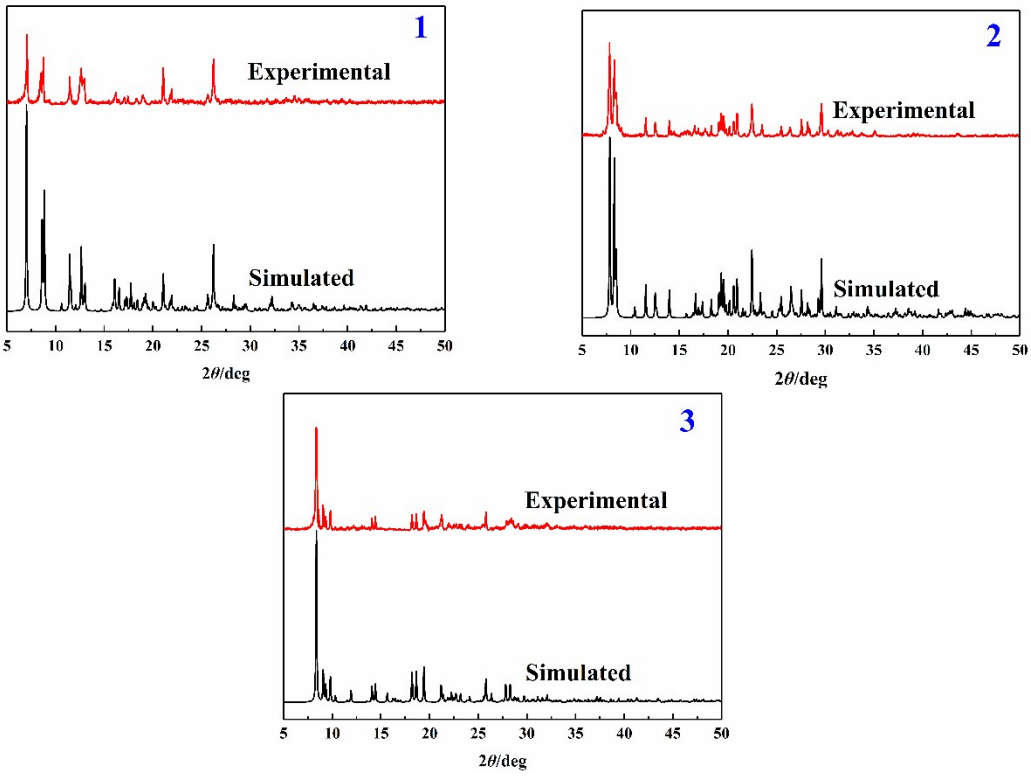

Fig. S5. The PXRD patterns of the bulk samples are consistent with the simulated ones of the single crystal structures in Cd-CPs **1**–**3.**

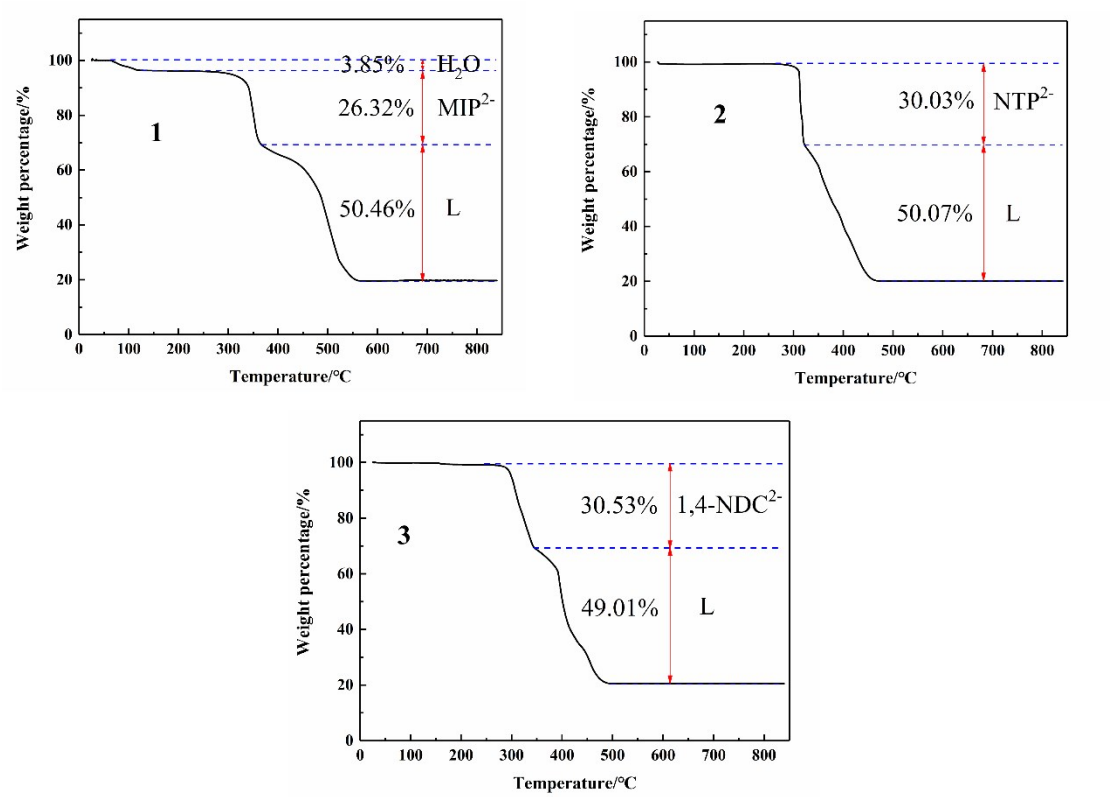

Fig. S6. TGA curves of Cd-CPs **1–3.**

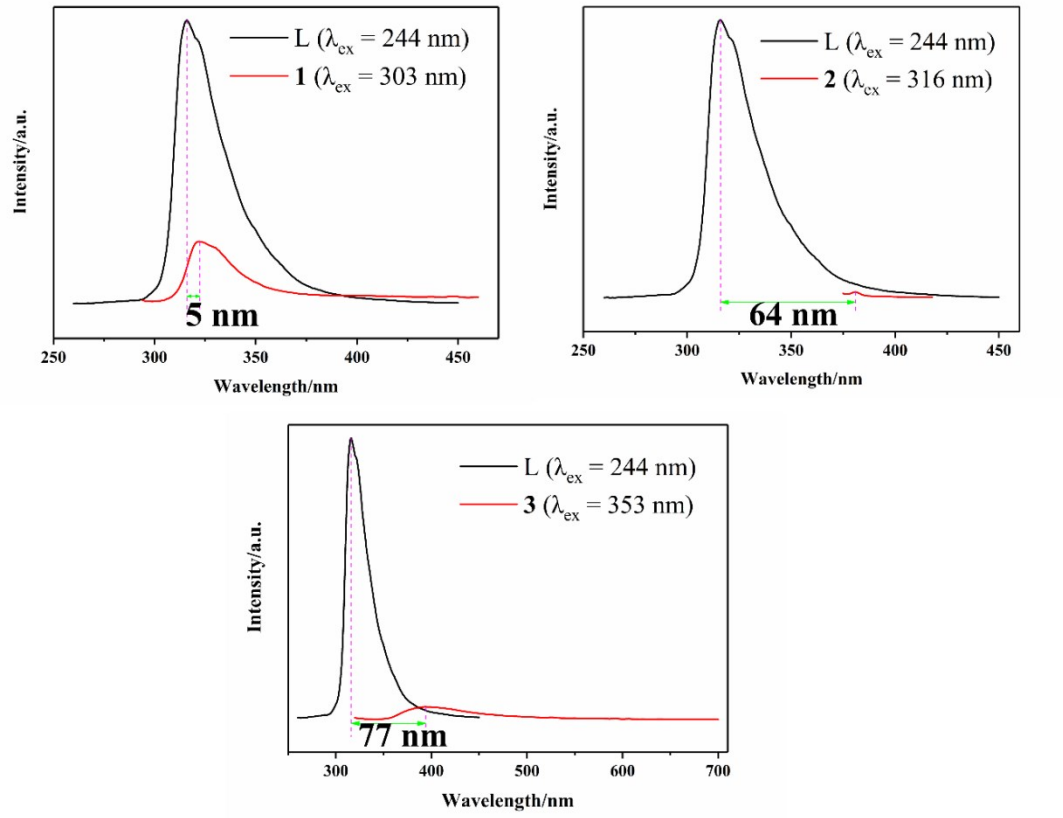

Fig. S7. Luminescence emission spectra of L and **1-3** in the solid state.

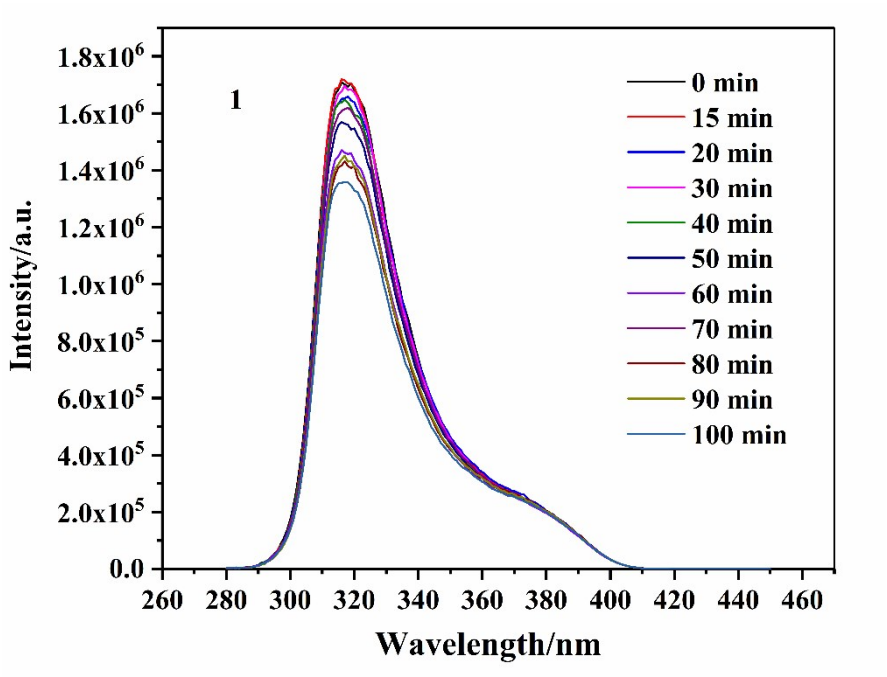

(a)

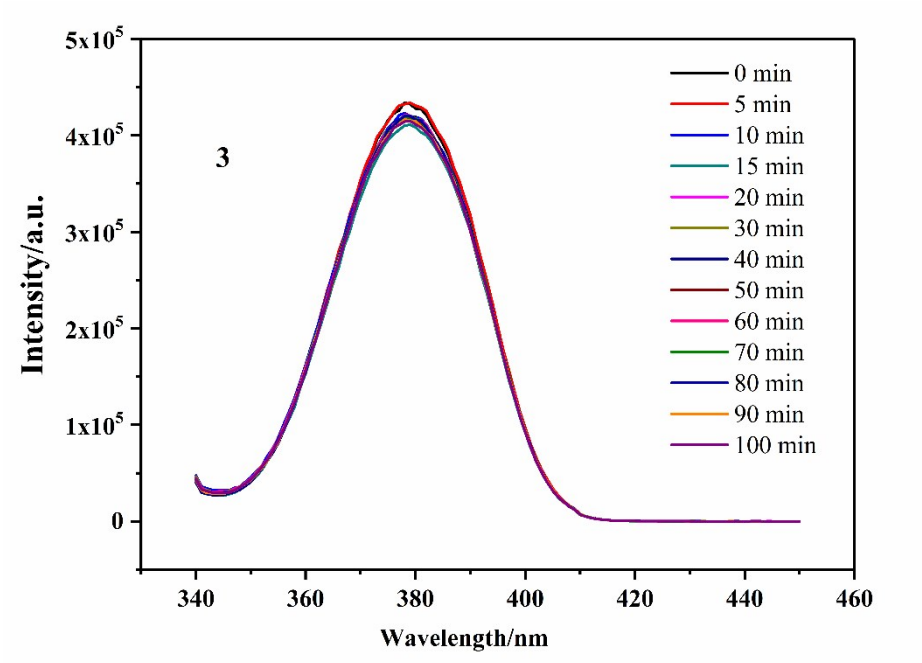

(b)

Fig. S8. (a) Time-dependent emission spectra of **1** suspended in aqueous solutions; (b) Time-dependent emission spectra of **3** suspended in aqueous solutions.

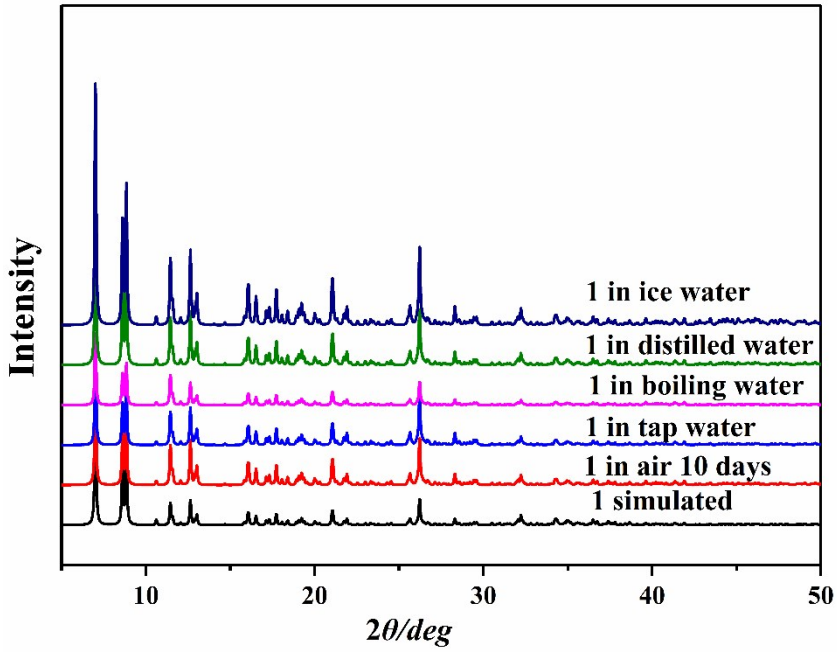

(a)

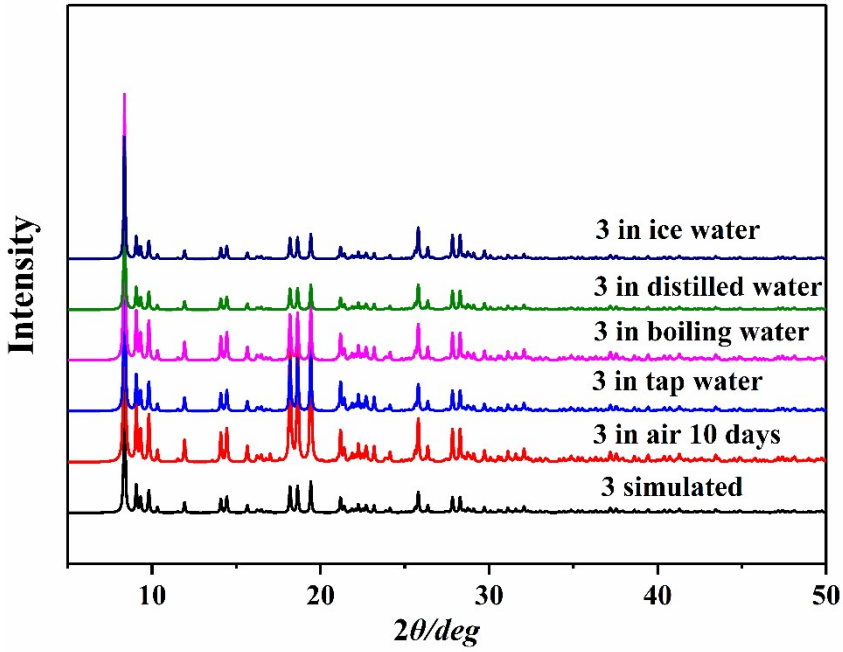

(b)

Fig. S9. (a) PXRD patterns of **1** under simulated conditions; (b)PXRD patterns of **3** under simulated conditions.

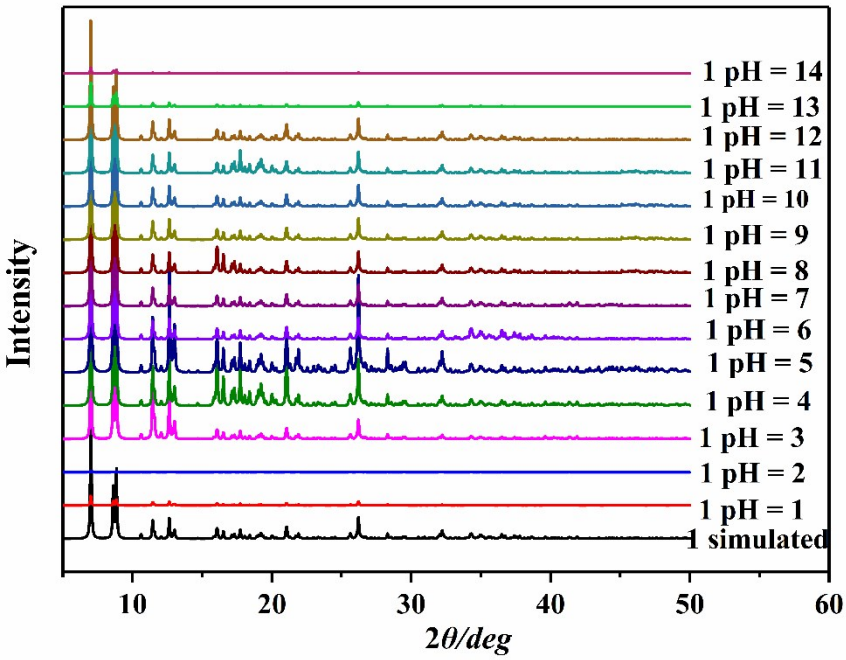

(a)

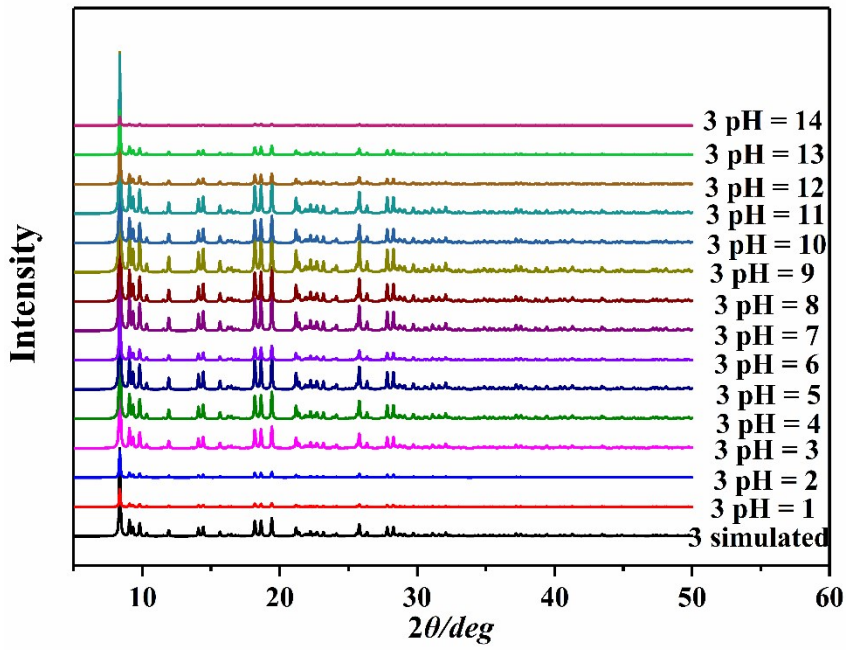

(b)

Fig. S10. (a) The change of the PXRD patterns of **1** in different pH solutions; (b) The change of PXRD patterns of **3** in different pH solutions.

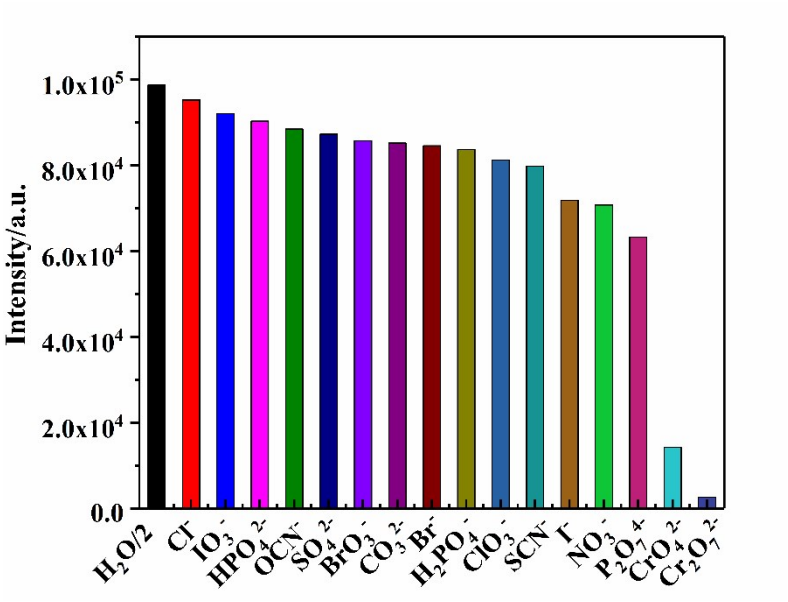

Fig. S11. Fluorescence intensities of **2** in water with various potassium salts (5×10^{-4} M).

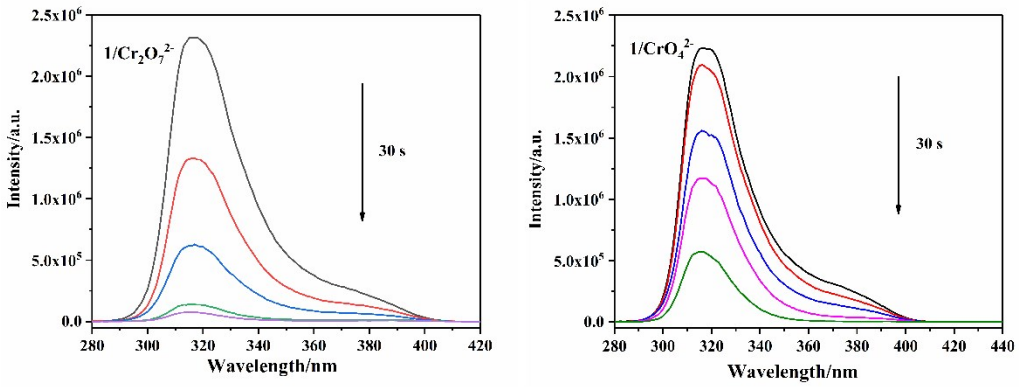

Fig. S12. In **1**, the time required for the quenching efficiency of $Cr_2O_7^{2-}$/CrO_4^{2-} anions to reach the maximum.

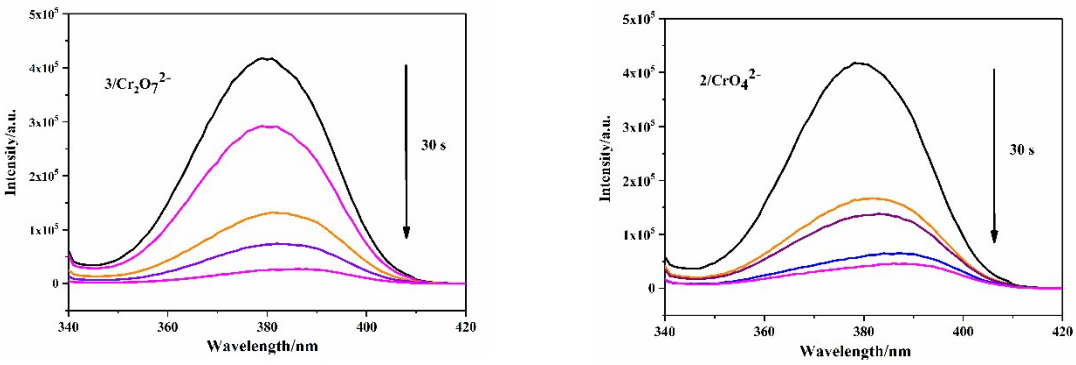

Fig. S13. In **3**, the time required for the quenching efficiency of $Cr_2O_7^{2-}$/CrO_4^{2-} anions to reach the maximum.

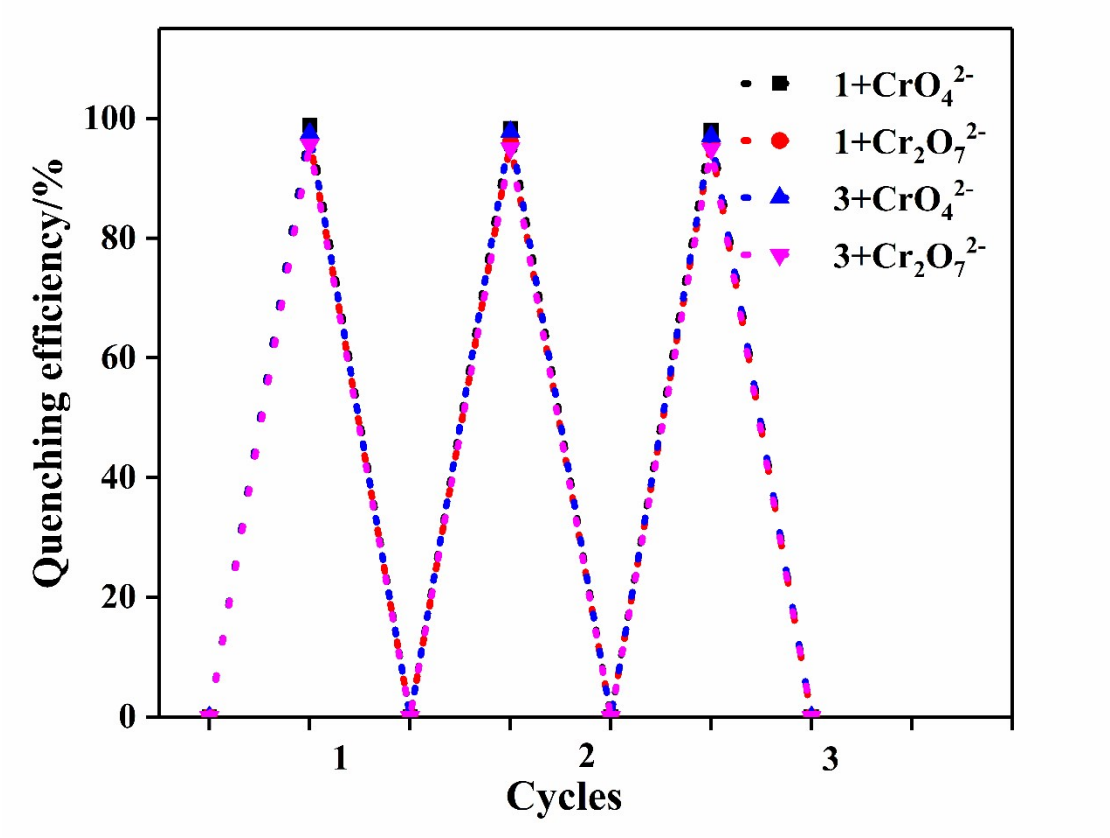

Fig. S14. Comparison of the quenching efficiency of **1** and **3** for $Cr_2O_7^{2-}$/CrO_4^{2-}over three cycles.

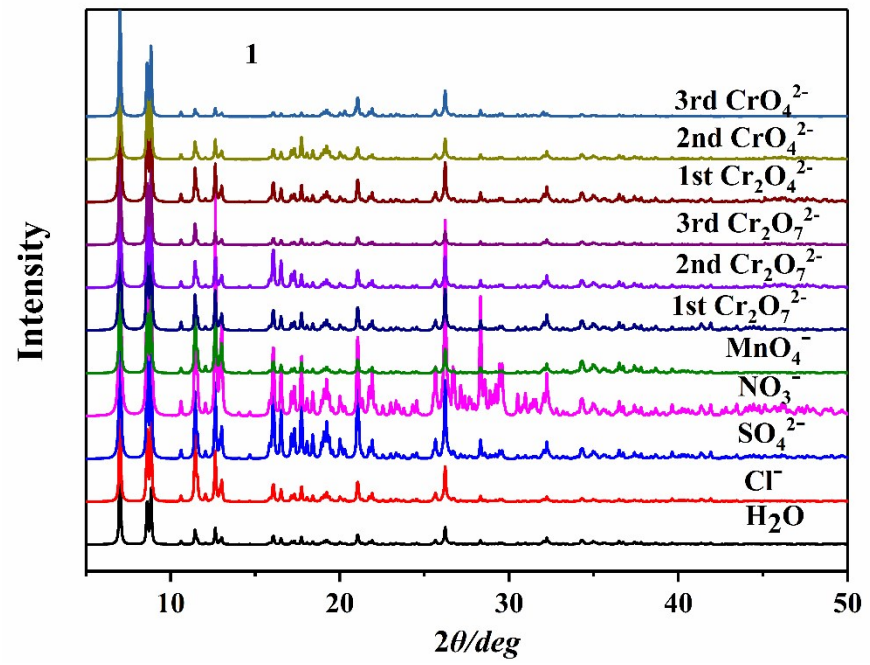

(a)

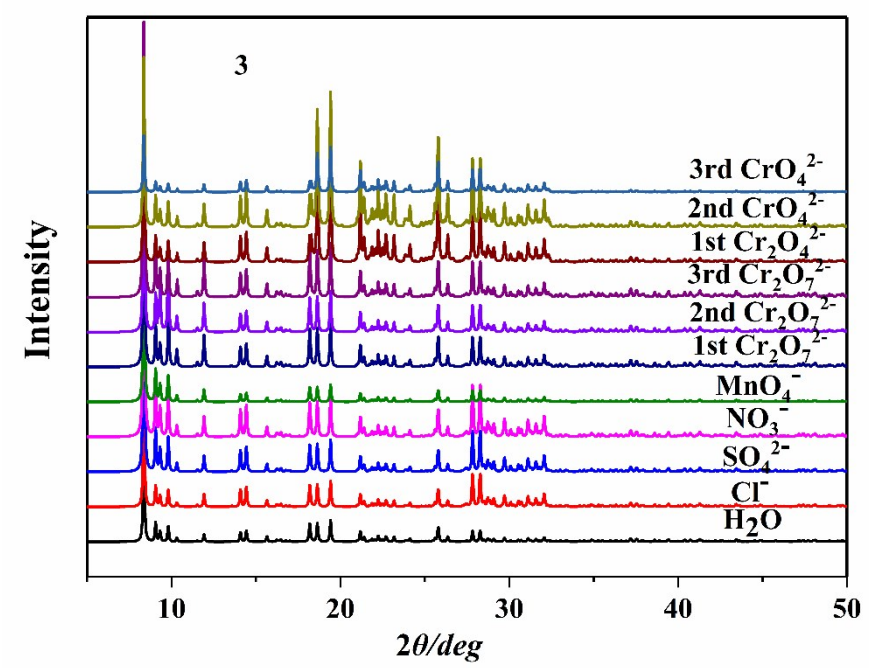

(b)

Fig. S15. (a)The PXRD patterns of **1** sample was immersed in H_2O solution containing $Cr_2O_7^{2-}/CrO_4^{2-}$ anions and other common anions; (b)The PXRD patterns of **3** sample was immersed in H_2O solution containing $Cr_2O_7^{2-}/CrO_4^{2-}$ anions and other common anions.

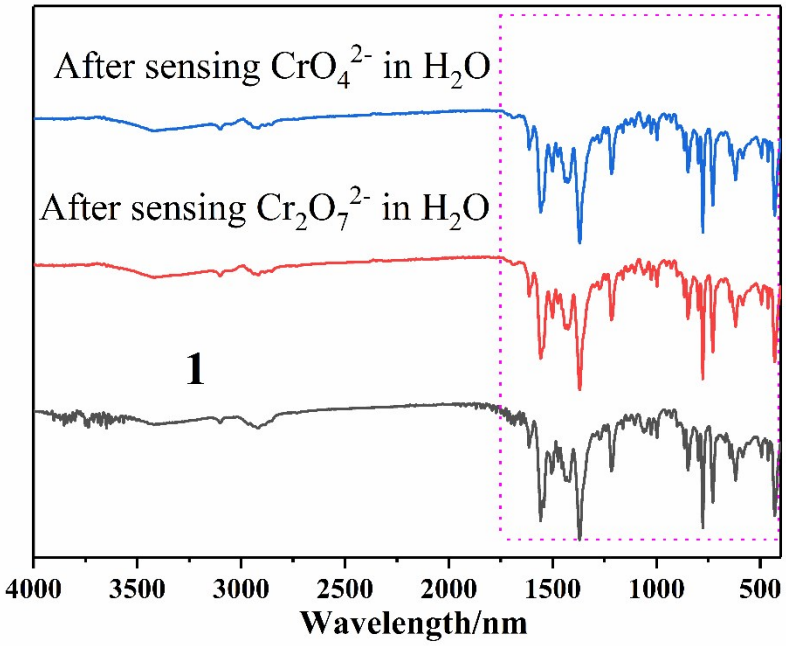

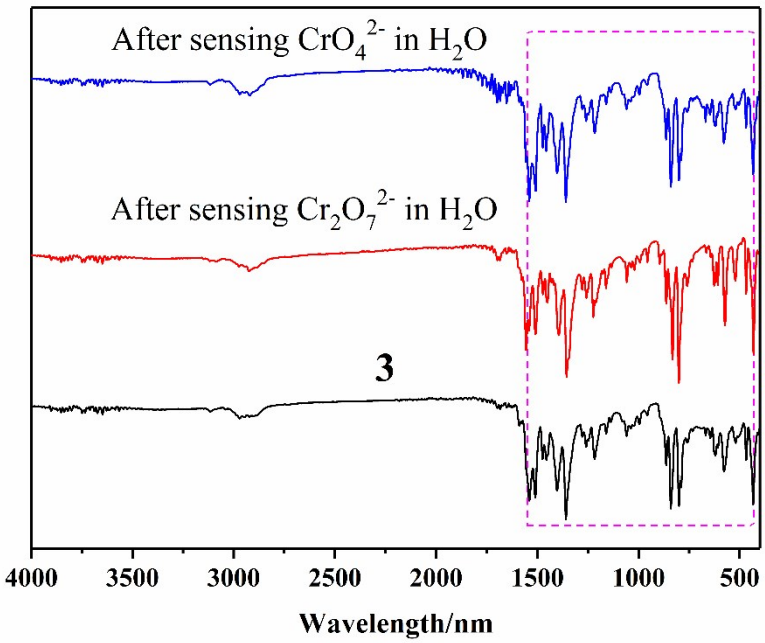

Fig. S16. (a)The original infrared spectrum of **1**, and the infrared spectra measured after $Cr_2O_7^{2-}$/CrO_4^{2-} detection of **1.** (b)The original infrared spectrum of **3**, and the infrared spectra measured after $Cr_2O_7^{2-}$/CrO_4^{2-} detection of **3.**

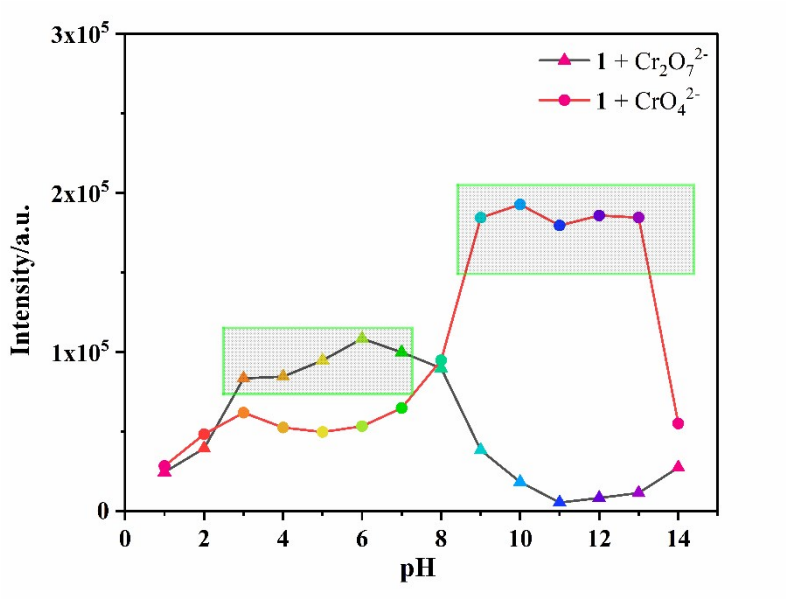

(a)

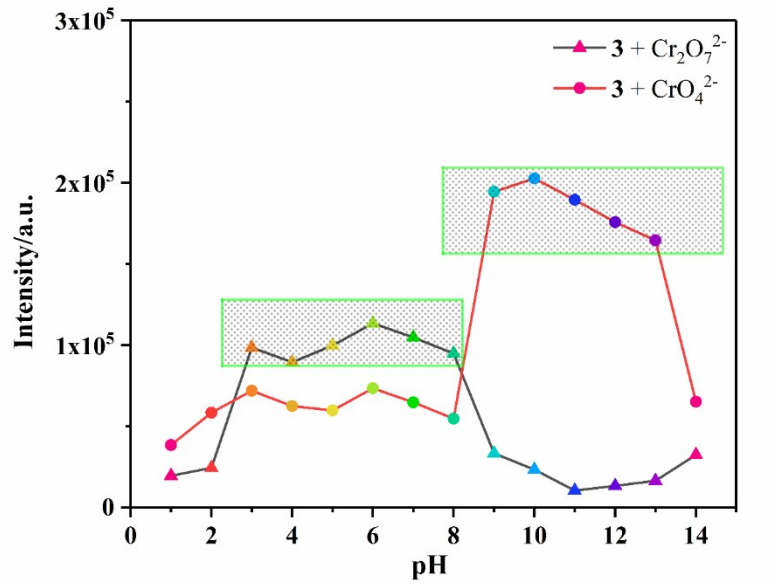

(b)

Fig. S17. (a) Effects of pH on the fluorescence maxima of **1** + CrO_4^{2-} (circle) and **1** + $Cr_2O_7^{2-}$ (triangle). Solvent: H_2O (1:1, v/v); (b) Effects of pH on the fluorescence maxima of **3** + CrO_4^{2-} (circle) and **3** + $Cr_2O_7^{2-}$ (triangle). Solvent: H_2O (1:1, v/v).

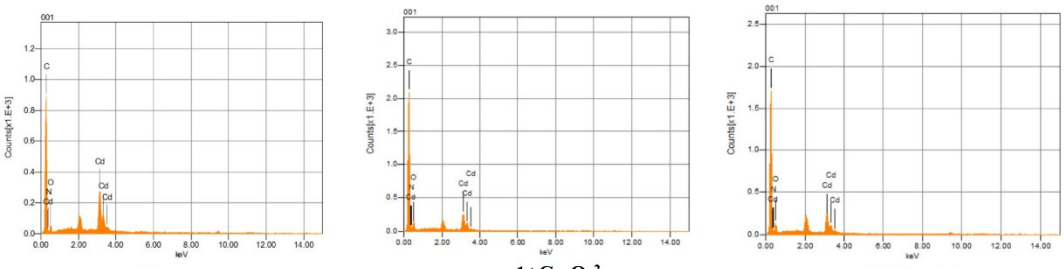

(a)

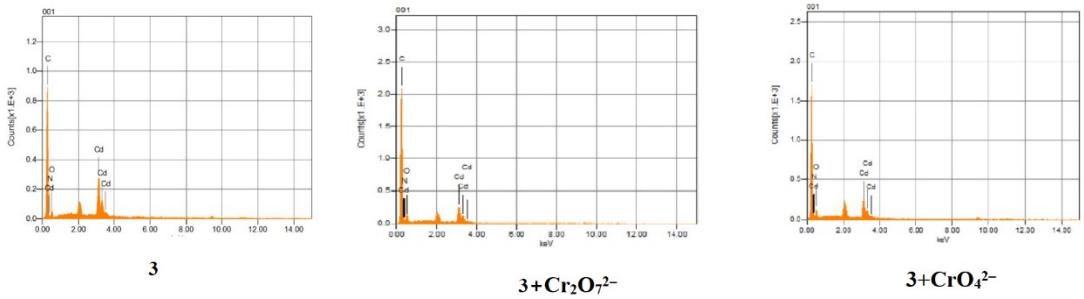

(b)

Fig. S18. (a) The EDX patterns of **1**, **1** + CrO_4^{2-}, **1** + $Cr_2O_7^{2-}$, respectively; (b) The EDX patterns of **3**, **3** + CrO_4^{2-}, **3** + $Cr_2O_7^{2-}$, respectively.

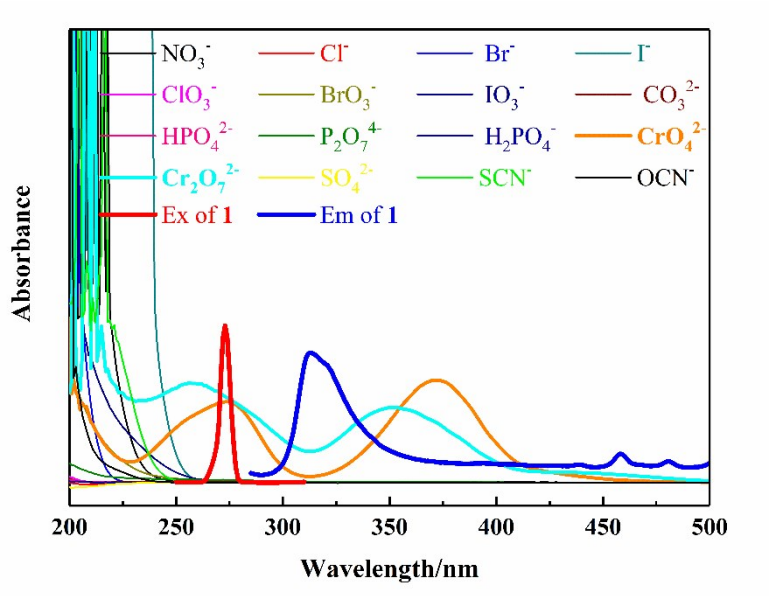

(a)

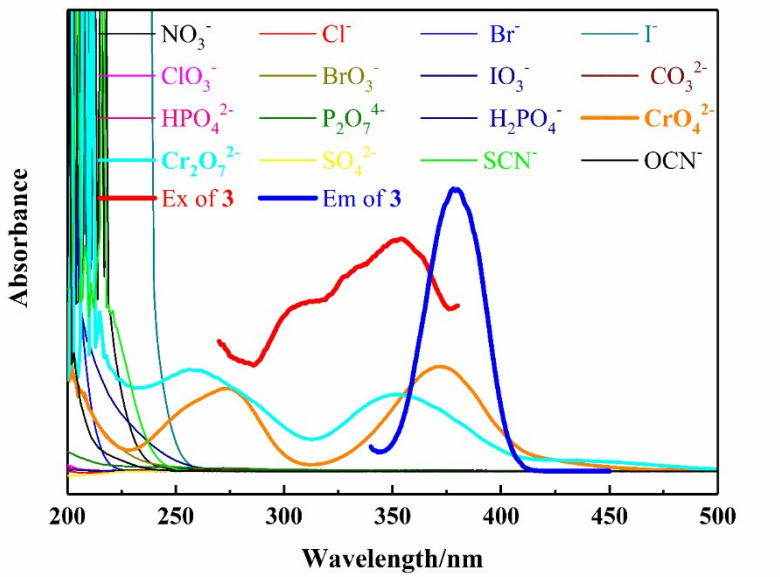

(b)

Fig. S19. (a) Spectral overlap between the absorption spectrum of $Cr_2O_7^{2-}$ anions and the excitation spectra of **1**; (b) Spectral overlap between the absorption spectrum of CrO_4^{2-}anions and the excitation spectra of **3**.